










Competing magnetic phases in the frustrated spin-1/2 chain compound β -TeVO₄ probed by NMR

M. Pregelj ^{1,*}, A. Zorko ^{1,2}, D. Arčon ^{1,2}, M. Klanjšek ¹, N. Janša ¹, P. Jeglič ¹,
O. Zaharko,³ S. Krämer ⁴, M. Horvatić ⁴, and A. Prokofiev ⁵

¹Jožef Stefan Institute, Jamova cesta 39, 1000 Ljubljana, Slovenia

²Faculty of Mathematics and Physics, University of Ljubljana, Jadranska u. 19, 1000 Ljubljana, Slovenia

³Laboratory for Neutron Scattering and Imaging, PSI, CH-5232 Villigen, Switzerland

⁴Laboratoire National des Champs Magnétiques Intenses, LNCMI-CNRS (UPR3228), EMFL, Université Grenoble Alpes, UPS and INSA Toulouse, Boîte Postale 166, 38042 Grenoble Cedex 9, France

⁵Institute of Solid State Physics, Vienna University of Technology, Wiedner Hauptstrasse 8-10, 1040 Vienna, Austria



(Received 7 April 2021; revised 17 November 2021; accepted 11 January 2022; published 26 January 2022)

In frustrated spin-1/2 chains the competition between the nearest- and next-nearest-neighbor exchange interactions leads to a rich phase diagram that becomes even richer in the presence of perturbations in their material realizations. These effects are still largely unexplored, so that new insight into static and dynamic magnetism, in particular by sensitive local probes, is highly desired. Here we present a comprehensive ¹⁷O nuclear magnetic resonance study of β -TeVO₄, where the anisotropy of the main exchange interactions and additional weak interchain exchange interactions complement the theoretical phase diagram. Our results confirm the dynamical nature of the intriguing spin-stripe phase that has been reported in previous studies. In addition, we find that the magnetic order in the high-field phase, which develops just below the magnetization saturation, is consistent with an unusual type of spin-density-wave (SDW) order with different alignments of the magnetic moments on the neighboring chains. This is reminiscent of the ordering in the SDW phase, realized in the absence of the magnetic field, and is thus most likely stabilized by magnetic anisotropy.

DOI: [10.1103/PhysRevB.105.035145](https://doi.org/10.1103/PhysRevB.105.035145)

I. INTRODUCTION

Frustrated spin-1/2 chains, i.e., chains with nearest- and next-nearest-neighbor Heisenberg exchange interactions, J_1 and J_2 , respectively, have been extensively studied [1–4] due to their rich phase diagram [5–7]. Recently, the focus has been on compounds with ferromagnetic J_1 [4,8–10], where a spin-nematic state, exhibiting long-range order of magnetic quadrupoles born out of magnon pairing [11–13], has been predicted [5–7]. Moreover, besides this enigmatic state, ferromagnetic-frustrated spin-1/2 chains show a plethora of other intriguing phases [5,6]. To begin with, the zero-field magnetic ground state is characterized by the long-range order of vector-chiral (VC) correlations. With increasing the magnetic field, a spin-density-wave (SDW) phase develops, which is characterized by incommensurate amplitude modulation of the ordered magnetic moments. Just below the magnetization saturation, the emergence of the spin-nematic state is anticipated, but its realization is in real systems typically hindered by perturbations, e.g., small additional intra or interchain interactions or magnetic anisotropy [4,14,15]. On the other hand, perturbations may lead to novel phases with intricate magnetic properties that further enrich the phase diagram of the frustrated spin-1/2 chain [16] and are yet to be explored experimentally.

An intriguing compound containing zigzag chains of magnetic V⁴⁺ ($S = 1/2$) ions is β -TeVO₄ [17]. This system exhibits a magnetic phase diagram [Fig. 1(a)] that matches very well the theoretical phase diagram of J_1 - J_2 spin-1/2 chain with ferromagnetic $J_1 \sim -38$ K and antiferromagnetic $J_2 \sim -J_1$ [18]. Yet, the exchange anisotropy and weak interchain interactions lead to some unexpected properties. The system orders below $T_{N1} = 4.6$ K, where the SDW phase develops, whereas the VC magnetic ground state is established below $T_{N3} = 2.3$ K. Between $T_{N2} = 3.3$ K and T_{N3} , however, an extraordinary spin-stripe phase emerges, where the two SDW order parameters that constitute the VC phase have different magnetic ordering vectors [18]. This phase is characterized by unusual spin dynamics in the MHz frequency range detected by muon spin relaxation [19], which still lacks an independent experimental confirmation. Applying the magnetic field at lowest temperatures induces the same spin-stripe phase between $B_{C1} \approx 2.5$ T and $B_{C2} \approx 5$ T, which is followed by the SDW phase at higher fields (Fig. 1). In the SDW phase the magnetic ordering vector monotonically decreases with increasing magnetic field [15], which complies with theoretical predictions [6]. However, this dependence is broken at $B_{C3} \approx 18$ T, where, instead of the anticipated spin-nematic phase, a high-field (HF) phase with yet unknown incommensurate dipolar magnetic order has been found [15,20].

Here we explore the magnetic phase diagram of β -TeVO₄ by ¹⁷O nuclear magnetic resonance (NMR). A previous low-magnetic-field NMR study [21] that focused on ¹²⁵Te nuclei was not able to probe the magnetism below ~ 10 K. This

*matej.pregelj@ijs.si

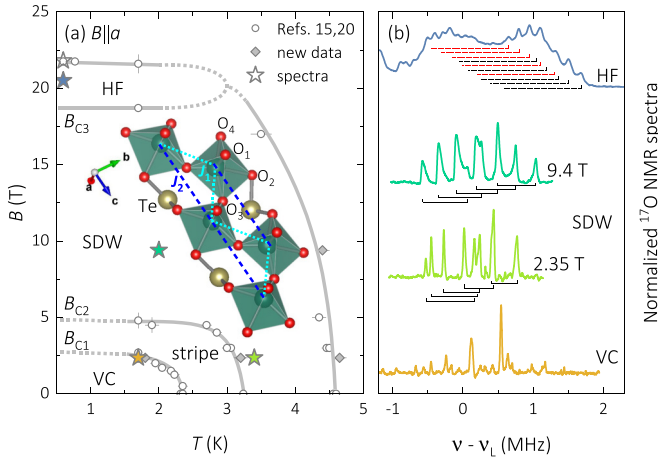


FIG. 1. (a) Magnetic phase diagram of β -TeVO₄ in magnetic field applied along the a crystallographic axis. Inset: A part of the V⁴⁺ ($S = 1/2$) zigzag chain, consisting of corner sharing VO₅ pyramids that include four crystallographically different O sites. J_1 is bridged by O atoms, whereas J_2 is bridged via O-Te-O paths. (b) ¹⁷O NMR spectra for the highest-frequency O site measured at different positions in the phase diagram [marked by corresponding stars of the same color in (a)]. The horizontal square brackets denote the U singularities corresponding to the same satellite line split by the incommensurate SDW order. Only one side of the bracket can be resolved in the HF phase.

was due to direct involvement of the Te ions in the main superexchange paths, leading to a very strong hyperfine interaction and consequent extremely rapid relaxation. In contrast to Te, one of four crystallographically inequivalent O sites experiences sufficiently small hyperfine fields, allowing us to successfully probe the NMR response also in the long-range-ordered magnetic phases. In fact, by extending the measurement range down to 0.5 K and up to 21.8 T, we are able to confirm the dynamical nature of the spin-stripe phase, reveal details about the high-field magnetic structure, and observe potential magnetic-field-induced closing of the magnon gap in the SDW phase. Our study, hereby, represents an important complementary insight into the magnetic properties of β -TeVO₄ and illuminates the influence of anisotropic interactions on magnetic phases in the J_1 - J_2 spin-1/2 chain compounds from a local perspective.

II. EXPERIMENT

The same single-crystal sample ($1.00 \times 3.10 \times 7.55$ mm³) was used as in our previous NMR study [20]. The crystal was grown by chemical vapor transport reaction using TeO₂ and VO₂ as starting materials and TeCl₄ as a transport agent. The enrichment of 8% ¹⁷O in the final product was achieved by a preceding partial oxidation of V₂O₃ to VO₂ by ¹⁷O₂. The ¹⁷O NMR was measured using a custom-built spectrometer at Jožef Stefan Institute, Slovenia, as well as a high-field spectrometer at the Laboratoire National des Champs Magnétiques Intenses (LNCMI), Grenoble, France, altogether covering the magnetic field, B , range between 2.3 and 24 T. The shape of the coil was adapted to fit the crystal (flat elongated plate), while a goniometer was used to adjust

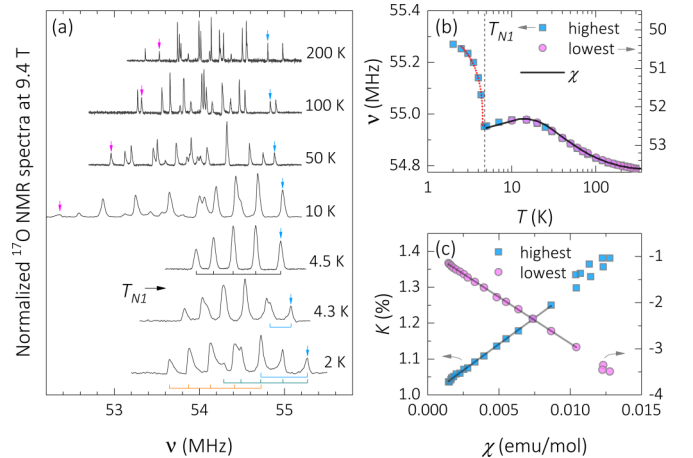


FIG. 2. (a) The temperature dependence of the ¹⁷O NMR spectrum measured at 9.4 T. The horizontal square brackets denote the U singularities corresponding to the highest-frequency satellite. Five-pointed forks denote individual quintets obtained by fit (see text for details). (b) Shift of the lowest- and highest-frequency satellite lines (symbols), marked by arrows in (a), in comparison to magnetic susceptibility data from Ref. [18]. The dotted line represents the $(T - T_{N1})^\beta$ model with $\beta = 0.37(3)$. (c) Clogston-Jaccarino plot for the lowest- and highest-frequency satellite lines above T_{N1} . Solid lines represent linear fits.

the orientation of the sample with respect to the magnetic field direction, which was limited to the crystallographic ab plane. The transverse magnetization M_\perp decay controlled by the spin-spin relaxation $1/T_2$ was measured with a standard Hahn-echo pulse sequence and fitted by a single-exponential function $\exp(-2\tau/T_2)$, where τ is the time between the $\pi/2$ and π pulses. The decay of the longitudinal magnetization M_z , driven by the spin-lattice relaxation $1/T_1$ was fitted to the expression for the outer-satellite line of a spin $I = 5/2$ nucleus [22]:

$$M_z(t) = M_0 - M_1 [1/35 \exp(-t/T_1) + 3/14 \exp(-3t/T_1) + 2/5 \exp(-6t/T_1) + 2/7 \exp(-10t/T_1) + 1/14 \exp(-15t/T_1)], \quad (1)$$

where t is the time after the initial inversion pulse, $M_0 = M_z(t \rightarrow \infty)$ the equilibrium magnetization, and $M_1 = M_0 - M_z(t = 0)$ the amplitude of the magnetization inversion.

III. RESULTS

To determine the coupling between the ¹⁷O nuclei and the magnetic moments of the magnetic ions as well as to obtain an overview of the magnetic behavior in the paramagnetic and SDW states, we first measured temperature dependence of the ¹⁷O NMR spectrum of β -TeVO₄ in the magnetic field $B = 9.4$ T applied along the crystallographic a axis, i.e., perpendicular to the VO₅ chains. At room temperature, the spectrum comprises 20 sharp peaks [Fig. 2(a)] corresponding to ¹⁷O ($I = 5/2$) quintets from four crystallographically inequivalent O sites split by quadrupole interaction. We note that some of the spectral lines overlap. On cooling, three quintets shift to lower frequencies while the fourth

quintet shifts to higher frequencies, i.e., in agreement with our high-field study [20]. This response becomes obvious when plotting the temperature dependence of the positions of two representative spectral lines [Fig. 2(b)] marked by arrows in Fig. 2(a). The two shifts are significantly different, as the line moving to lower frequencies shifts approximately seven times more than the one shifting to higher frequencies, indicating substantially weaker hyperfine coupling for the latter. Both shifts exhibit a pronounced maximum at ~ 12.7 K, perfectly matching the temperature dependence of the magnetic susceptibility χ [Fig. 2(b)]. In fact, plotting the magnetic hyperfine, i.e., Knight, shift $K = (\nu - \nu_L)/\nu_L$, where $\nu_L = {}^{17}\text{O}$ gyromagnetic ratio and B is the applied magnetic field, as a function of χ , i.e., the so-called Clogston-Jaccarino plot [Fig. 2(c)], we find a clear linear dependence, where the slope is directly proportional to the strength of the hyperfine interactions [23]. The derived hyperfine couplings for $B||a$ are $A_{\text{low}} = -1.12(2) \text{ T}/\mu_B$ and $A_{\text{high}} = 0.163(2) \text{ T}/\mu_B$ for the low and the high frequency sites, respectively. The bigger value is comparable with the values derived for the ${}^{125}\text{Te}$ NMR amounting up to $5.8 \text{ T}/\mu_B$ [21], leading to a similar loss of the NMR signal below 10 K. The other coupling value is approximately seven times smaller, which explains why this site could be used for the low-temperature NMR study.

On further cooling, the spectral lines shifting to lower frequencies loose intensity and finally disappear below ~ 7 K [Fig. 2(a)], which is due to extremely fast spin-spin (T_2) relaxation driven by stronger hyperfine couplings of these lines compared to the lines that shift to higher frequencies. Consequently, at 4.5 K, i.e., just above the magnetic transition, the NMR spectrum reduces to only five lines, namely, a single quintet corresponding to the O site with the weakest hyperfine coupling. This particular O site is most likely the apical O_1 site that is isolated from the main exchange pathways [inset in Fig. 1(a)]. Below T_{N1} , each of the five lines broadens into a U-shaped spectrum [Fig. 2(a)], characteristic of incommensurate amplitude-modulated magnetic order in the SDW phase with the width of the U splitting determined by the amplitude of the projection of the magnetic-moments modulation on the external magnetic field. The position of the outer satellite line below T_{N1} [Fig. 2(b)], therefore, reflects the amplitude of the ordered magnetic moments in the SDW phase, which scales with temperature as $(T - T_{N1})^\beta$, yielding $\beta = 0.37(3)$ [see Figs. 2(b) and 3(c)]. This value is in agreement with the critical exponents for the order parameter in three-dimensional (3D) spin lattices, ranging from 0.33 to 0.36 for the Ising and Heisenberg cases, respectively, [24,25]. Indeed, the 3D nature of critical correlations is in line with the existence of sizable interchain, i.e., 3D, interactions identified in previous studies [26,27].

To explore all the low-field-ordered phases in the same applied field, we performed additional ${}^{17}\text{O}$ NMR measurements at 2.35 T. The temperature dependence of the spectrum measured below 5 K is shown in Fig. 3(a). The relative positions of the five spectral lines of the remaining quintet are significantly different from those collected at 9.4 T. This is a consequence of the ${}^{17}\text{O}$ Larmor frequency at 2.35 T being strongly affected by the quadrupolar interaction [28], determined by the ${}^{17}\text{O}$ quadrupolar moment and the local

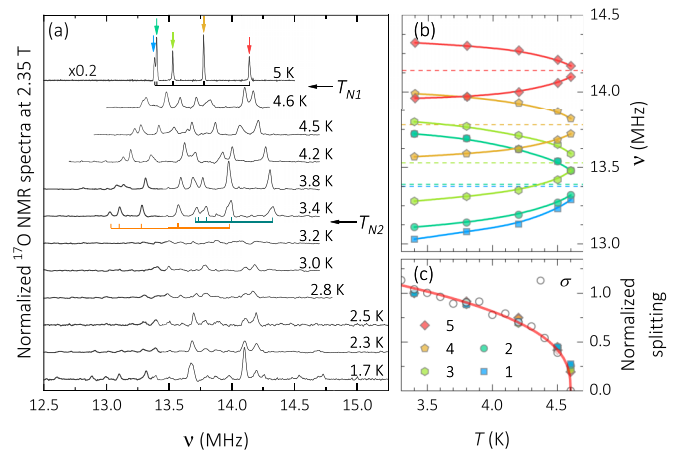


FIG. 3. (a) The temperature dependence of the ${}^{17}\text{O}$ NMR spectrum measured at 2.35 T at low temperatures. Five-pointed forks denote individual quintets obtained by fit (see text for details). (b) The peak frequencies demonstrating the splitting of the five spectral lines due to the establishment of the incommensurate magnetic order. Solid lines are guides to the eye. Colored dashed lines mark the positions of the spectral lines in the paramagnetic state at 5 K marked by arrows in (a). (c) The temperature dependence of the normalized NMR splittings (solid symbols) compared to the magnetic order parameter σ derived from neutron diffraction (empty symbols) [19]. The solid line is the fit of the $(T - T_{N1})^\beta$ model, with $\beta = 0.37(3)$.

electric-field-gradient (EFG) tensor. Nevertheless, below T_{N1} , similarly as for measurements at 9.4 T, also at 2.35 T each of the five lines splits into two that monotonically shift away from each other on cooling [Fig. 3(b)], as expected for the SDW, i.e., amplitude-modulated, phase [29]. In fact, the temperature dependence of the U splitting [Fig. 3(c)] follows the same $(T - T_{N1})^\beta$ dependence as the outer satellite at 9.4 T [Fig. 2(b)], while both dependencies exactly match the evolution of the magnetic order parameter obtained from neutron diffraction at zero field [Fig. 3(c)] [19].

A detailed inspection of the U split lines in the SDW phase [Fig. 1(b)] provides further insight into quadrupolar effects. Namely, while the U splittings of different lines in the quintets are rather similar at 9.4 T, they differ significantly at 2.35 T, yet again indicating that quadrupolar effects at 2.35 T are strong and that first-order perturbation theory no longer applies. It is thus convenient to consider the edge singularities of the U-shaped lines as two quintets corresponding to two magnetically inequivalent O_1 sites; one that on cooling shifts to higher and one that shifts to lower frequencies [Figs. 2(a) and 3(a)]. The observed behavior can then be described by exact diagonalization of the quadrupolar Hamiltonian $H = \hbar\gamma \mathbf{I} \cdot \mathbf{B}_{\text{eff}} + h\nu_Q [3I_z^2 - I(I+1) + \eta(I_+^2 + I_-^2)/2]/6$, where h is the Planck constant, $\hbar = h/2\pi$, $\mathbf{I} = (I_x, I_y, I_z)$ is the nuclear spin vector, $I_\pm = I_x \pm iI_y$, \mathbf{B}_{eff} is the effective magnetic field, ν_Q is the quadrupolar frequency, and η is the EFG asymmetry parameter [30]. Adjusting ν_Q , η as well as the orientation and the size of \mathbf{B}_{eff} , we can exactly reproduce the two quintets measured in the paramagnetic phase, i.e., at 5 K, in the field of 2.35 and 9.4 T as well as the four (two in 2.35 T and two in 9.4 T) quintets in the SDW phase [five-pointed forks in Figs. 2(a) and 3(a)]. The derived parameters are

$\nu_Q = 1.05(5)$ MHz, $\eta = 0.62(5)$, and the orientations of the two principal EFG axes pointing along $(0.7, 0, -0.7)$ and $(0.5, 0.7, 0.5)$ in the a^*bc crystallographic system, which is in line with the fact that the O_1 local environment possesses no symmetry restrictions on the EFG tensor. We note that in our calculations a misalignment of $\sim 3^\circ$ between different experiments has been considered. Besides, we find that the local fields for the U edge singularities in the SDW phase deviate almost symmetrically from the paramagnetic value by $\sim \pm 0.05$ T in size and $\sim \pm 2^\circ$ in orientation. Considering the hyperfine coupling constant A_{high} this suggests that the amplitude of the modulated magnetic moments is $\sim 0.3 \mu_B$, i.e., in agreement with the neutron diffraction results [31]. We stress that the obtained parameters are not exact and should be refined by more involved angular-dependent measurements, yet they still provide a reasonable estimate of the EFG strength at the O_1 site. Finally, we point out that, in contrast to the results at 9.4 T, the U-shape of the spectral lines at 2.35 T is much less pronounced, as edge singularities are far more dominant, indicating that the middle parts of the spectrum associated with the reduced static magnetic moments are suppressed. This can be explained by enhanced T_2 relaxation, driven phason excitations of the SDW order [32,33], that have for small wave vectors (for the NMR case) a most pronounced effect on the reduced magnetic moments, i.e., on the middle of the U spectrum.

At the transition into the spin-stripe phase, i.e., at T_{N2} , the spectrum dramatically changes. The signal is almost completely lost, reflecting even stronger T_2 relaxation, which corroborates the dynamical nature of the spin-stripe phase on the MHz timescale [19]. We note that the spectra in Fig. 3(a) were measured with the shortest possible $\tau = 20 \mu\text{s}$ allowed by our spectrometer. On further cooling, some spectral features reappear, exhibiting an extended array of singularities at the lowest accessible temperature of 1.7 K. However, this temperature point lies at the border between the spin-stripe and the VC phase, so the resulting spectrum does not fully represent the magnetic order in the VC phase. Hence, based on the obtained spectrum, we cannot learn much about the VC phase, except for the fact that the T_2 relaxation in this phase is slowing down, supporting the static long-range order in this phase. Next, we explore the spin dynamics through the temperature dependencies of the spin-lattice and the spin-spin relaxation rates, $1/T_1$ and $1/T_2$, respectively. Both relaxation rates were measured for the outer satellite line [marked by the blue arrow in Fig. 2(a)], i.e., the line corresponding to the $m = -5/2$ to $m = -3/2$ transition [Fig. 4(c)]. Above the magnetic transition, the nuclear magnetization curves [Figs. 4(a) and (b)] yield well-defined and almost temperature-independent $1/T_1$ and $1/T_2$, as expected for a paramagnet with strong antiferromagnetic correlations [34]. In fact, the temperature independence of the $T_1/T_2 \approx 7$ [inset in Fig. 4(c)] ratio suggests that the T_2 relaxation is driven by fluctuations of nearby electronic spins, i.e., by the Redfield process [35,36], yielding

$$T_{2z}^{-1} = \frac{1}{2}(T_{1x}^{-1} + T_{1y}^{-1} - T_{1z}^{-1})|_{\omega=0} + [I(I+1) - m(m-1) - 1/2]T_{1z}^{-1}(\omega). \quad (2)$$

Taking $m = 5/2$, as the relaxation rates were measured on the outer satellite, the second term in Eq. (2) yields a prefactor

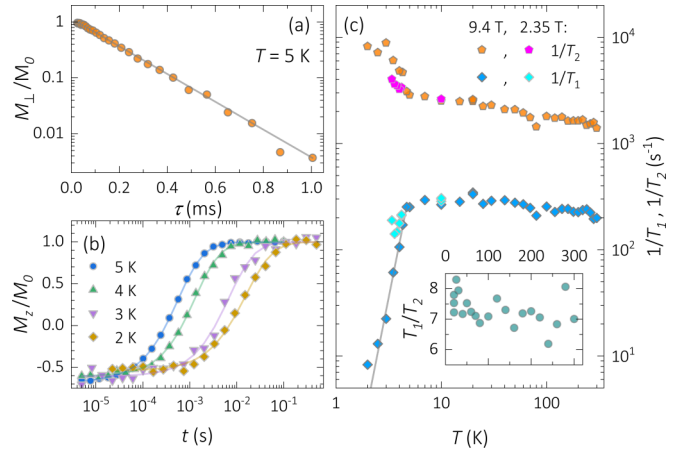


FIG. 4. A representative low-temperature (a) T_2 and (b) T_1 measurements (symbols), i.e., transverse- and longitudinal-magnetization (M_\perp and M_z) decays, respectively, for the highest-frequency satellite of the only-remaining low-temperature O site measured at 9.4 T and the corresponding fits (lines; see text). (c) The temperature dependence of the spin-lattice and the spin-spin relaxation rates, $1/T_1$ and $1/T_2$, respectively, measured for the highest-frequency satellite. The solid line shows a fit of the $1/T_1 \propto T^5$ model. Inset: The temperature dependence of T_1/T_2 .

of 4.5, which suggests that the $\omega = 0$ contribution [the first term in Eq. (2)] is rather anisotropic, implying $T_{1x}^{-1} + T_{1y}^{-1} \approx 6T_{1z}^{-1}$. This can be due to the anisotropy of the spin fluctuations as well as that of the hyperfine couplings since both contributions are allowed by a low symmetry of the O_1 site. In addition, the measurements at 2.35 T [Fig. 4(c)] show that the relaxation times at 10 K are the same as those obtained at 9.4 T. This indicates that, in the paramagnetic state, the relaxation processes are nearly frequency independent, which is indeed expected in the extreme-narrowing limit ensured by strong antiferromagnetic correlations.

At T_{N1} , the temperature-independent trend is abruptly broken, as on further cooling $1/T_1$ decreases proportional to T^p with $p = 5.0(2)$ for 9.4 T [solid line in Fig. 4(c)]. The T^5 dependence of $1/T_1$ has been observed in several quasi-one-dimensional spin systems [37,38] and is, in fact, predicted for a three-magnon process for $T \gg \Delta$, where Δ is the excitation gap of magnons [39]. The fact that the neutron scattering experiment in the absence of the magnetic field revealed a magnon gap of ~ 7 K (0.6 meV) (see Supplementary Material to Ref. [19]) suggests that this gap is almost completely closed by the applied magnetic field of 9.4 T (~ 6.3 K), pushing the system into the limit $T \gg \Delta$ in agreement with our NMR experiment. On the other hand, $1/T_2$ below T_{N1} gradually increases, which indicates slowing down of the spin-spin relaxation due to the establishment of long-range magnetic ordering. We note that the data collected at 2.35 T exhibit less pronounced temperature dependencies than at 9.4 T and are most likely affected by the proximity of the T_{N2} magnetic transition [Fig. 1(a)], occurring less than 1.5 K below T_{N1} . Moreover, at 2.35 T we were unable to consistently measure relaxation times below T_{N2} , as there is no distinct spectral feature [Fig. 3(a)] that would allow for reliable measurements at the same

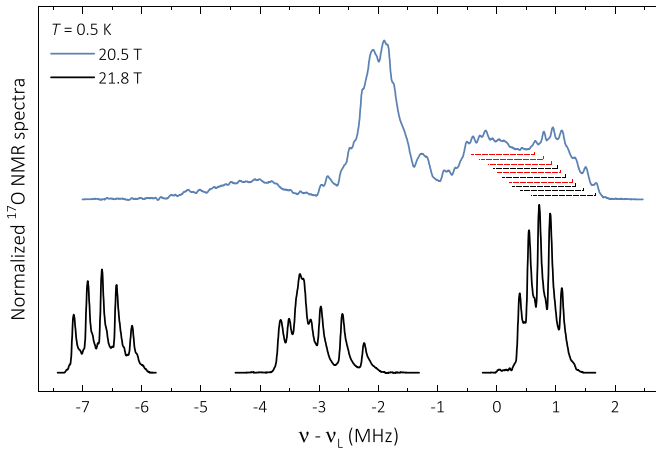


FIG. 5. ^{17}O NMR spectra measured in high-magnetic fields in the incommensurate HF phase and in the saturated state.

NMR transition. At last, we point out the absence of critical fluctuations in the paramagnetic state just above the T_{N1} transition. Considering a low symmetry of the O_1 site [inset in Fig. 1(a)] [17], a symmetry-based filtration of critical fluctuations is highly unlikely thus implying that the critical region is very narrow, i.e., in line with a 3D nature of the T_{N1} magnetic transition. Finally, we performed ^{17}O NMR also in high magnetic fields at 0.5 K. We measured NMR spectra in the HF phase, i.e., at 20.5 T, as well as above the magnetization saturation, at 21.8 T (Fig. 5). This complements the data from our previous study [20], where spectra were measured at fixed frequency by sweeping the magnetic field. Clearly, the T_2 relaxation at these fields is significantly reduced, as in the saturated phase all four quintets are observed again. Three quintets are found below the Larmor frequency, ν_L , while one quintet is found above ν_L , in agreement with the response observed in the paramagnetic phase at 9.4 T. Moreover, the large separation of the quintets at 21.8 T allows us to distinguish the difference in the EFG strengths at different oxygen sites, which are responsible for the splittings of the lines within the individual quintets. In particular, for $B||a$, these splittings amount to $\sim 0.25, 0.13, 0.35,$ and 0.19 MHz for the O sites sorted from the lowest to the highest frequency, respectively. We note, however, that these values reflect the EFG strengths along the applied magnetic field, i.e., along the a axis, and can change significantly for different field orientation.

In the HF phase, however, the contributions from the four O sites overlap. In particular, the low-frequency part of the spectrum is a complex mixture of several overlapping contributions that cannot be disentangled. On the other hand, the highest-frequency U-shaped feature [Fig. 1(b)] is most likely associated with the high-frequency O site (assigned to O_1 site). In fact, it appears that this part of the spectrum is composed of two sets of overlapping U-split quintets [Fig. 1(b)], which might develop due to the symmetry reduction of the magnetic order in the HF phase. Namely, the two neigh-

boring chains probably exhibit different alignments of the SDW-modulation eigenaxes, which would lead to different projections of the magnetic moments on the external magnetic field. A similar ordering was found by neutron diffraction in the SDW phase in the absence of the magnetic field [31], where magnetic moments lie along the a axis on one chain and along the c axis on the other. The possible similarity between the orders in these two phases is also supported by the fact that both phases exhibit similar magnetic ordering vectors [15], highlighting the importance of the magnetic anisotropy in this system.

IV. SUMMARY AND CONCLUSION

By employing ^{17}O nuclear magnetic resonance (NMR), we investigated the magnetic properties of $\beta\text{-TeVO}_4$ for $B||a$. We determined the hyperfine coupling constants for the two out of four crystallographically different O sites, i.e., the two that exhibit the smallest and the largest frequency shifts, which differ by a factor of ~ 7 . The shift of one ^{17}O quintet is considerably smaller than those of the other three, implying that it probably corresponds to the isolated O_1 site, positioned on the top of the VO_5 pyramid. For this site, we also estimated the local EFG tensor. In addition, we determined the critical exponent for the magnetic order parameter, $\beta = 0.37(3)$, which is in agreement with the theoretical predictions for 3D spin models, and thus corroborates sizable interchain interactions [27]. Furthermore, in the spin-stripe phase we confirmed the presence of strong dynamics in the MHz range that is driven by the unusual low-energy bound-phason excitations emerging due to a weak forth-order exchange coupling term [19]. On the other hand, in the SDW phase, the temperature dependence of the $1/T_1$ relaxation at 9.4 T exhibits the T^5 dependence, implying that the magnon gap in this phase is almost completely closed by the applied magnetic field. Finally, the U shape of the high-frequency part of the spectrum in the HF phase suggests that the neighboring chains might exhibit different alignments of the magnetic moments, similarly as found in the zero-field VC magnetic ground state. Still, detailed understanding of the HF phase calls for future density-functional-theory calculations of the EFG tensors at all O sites, which would allow for more involved modeling of the HF NMR spectrum. For such calculations the derived hyperfine-coupling constants and EFG parameters should serve as an important point of reference, allowing an independent verification of the calculation precision.

ACKNOWLEDGMENTS

This work has been funded by the Slovenian Research Agency (Projects No. J1-9145, No. J1-2461, No. N1-0148, and No. J2-2513, and Program No. P1-0125) and the Swiss National Science Foundation (project SCOPES IZ73Z0_152734/1). We acknowledge the support of the LNCMI-CNRS, member of the European Magnetic Field Laboratory (EMFL).

[1] G. Castilla, S. Chakravarty, and V. J. Emery, Quantum Magnetism of CuGeO_3 , *Phys. Rev. Lett.* **75**, 1823 (1995).

[2] S. Seki, Y. Yamasaki, M. Soda, M. Matsuura, K. Hirota, and Y. Tokura, Correlation Between Spin Helicity and an Electric

- Polarization Vector in Quantum-Spin Chain Magnet LiCu_2O_2 , *Phys. Rev. Lett.* **100**, 127201 (2008).
- [3] S. Nishimoto, S.-L. Drechsler, R. O. Kuzian, J. van den Brink, J. Richter, W. E. A. Lorenz, Y. Skourski, R. Klingeler, and B. Büchner, Saturation Field of Frustrated Chain Cuprates: Broad Regions of Predominant Interchain Coupling, *Phys. Rev. Lett.* **107**, 097201 (2011).
- [4] E. Cemal, M. Enderle, R. K. Kremer, B. Fåk, E. Ressouche, J. P. Goff, M. V. Gvozdkova, M. E. Zhitomirsky, and T. Ziman, Field-Induced States and Excitations in the Quasicritical Spin-1/2 Chain Linarite, *Phys. Rev. Lett.* **120**, 067203 (2018).
- [5] T. Hikihara, L. Kecke, T. Momoi, and A. Furusaki, Vector chiral and multipolar orders in the spin-1/2 frustrated ferromagnetic chain in magnetic field, *Phys. Rev. B* **78**, 144404 (2008).
- [6] J. Sudan, A. Lüscher, and A. M. Läuchli, Emergent multipolar spin correlations in a fluctuating spiral: The frustrated ferromagnetic spin-1/2 Heisenberg chain in a magnetic field, *Phys. Rev. B* **80**, 140402(R) (2009).
- [7] T. Hikihara, T. Momoi, A. Furusaki, and H. Kawamura, Magnetic phase diagram of the spin-1/2 antiferromagnetic zigzag ladder, *Phys. Rev. B* **81**, 224433 (2010).
- [8] M. Mourigal, M. Enderle, B. Fåk, R. K. Kremer, J. M. Law, A. Schneidewind, A. Hiess, and A. Prokofiev, Evidence of a Bond-Nematic Phase in LiCuVO_4 , *Phys. Rev. Lett.* **109**, 027203 (2012).
- [9] B. Willenberg, M. Schäpers, A. U. B. Wolter, S.-L. Drechsler, M. Reehuis, J.-U. Hoffmann, B. Büchner, A. J. Studer, K. C. Rule, B. Ouladdiaf, S. Süllow, and S. Nishimoto, Complex Field-Induced States in Linarite $\text{PbCuSO}_4(\text{OH})_2$ with a Variety of High-Order Exotic Spin-Density Wave States, *Phys. Rev. Lett.* **116**, 047202 (2016).
- [10] A. Orlova, E. L. Green, J. M. Law, D. I. Gorbunov, G. Chanda, S. Krämer, M. Horvatić, R. K. Kremer, J. Wosnitzer, and G. L. J. A. Rikken, Nuclear Magnetic Resonance Signature of the Spin-Nematic Phase in LiCuVO_4 at High Magnetic Fields, *Phys. Rev. Lett.* **118**, 247201 (2017).
- [11] A. V. Chubukov, Chiral, nematic, and dimer states in quantum spin chains, *Phys. Rev. B* **44**, 4693 (1991).
- [12] N. Shannon, T. Momoi, and P. Sindzingre, Nematic Order in Square Lattice Frustrated Ferromagnets, *Phys. Rev. Lett.* **96**, 027213 (2006).
- [13] M. E. Zhitomirsky and H. Tsunetsugu, Magnon pairing in quantum spin nematic, *Europhys. Lett.* **92**, 37001 (2010).
- [14] A. A. Bush, N. Büttgen, A. A. Gippius, M. Horvatić, M. Jeong, W. Kraetschmer, V. I. Marchenko, Y. A. Sakhmatov, and L. E. Svistov, Exotic phases of frustrated antiferromagnet LiCu_2O_2 , *Phys. Rev. B* **97**, 054428 (2018).
- [15] M. Pregelj, A. Zorko, M. Klanjšek, O. Zaharko, J. S. White, O. Prokhnenko, M. Bartkowiak, H. Nojiri, H. Berger, and D. Arčon, Magnetic ground state of the frustrated spin- $\frac{1}{2}$ chain compound $\beta\text{-TeVO}_4$ at high magnetic fields, *Phys. Rev. B* **100**, 094433 (2019).
- [16] H. Ueda and S. Onoda, Roles of easy-plane and easy-axis XXZ anisotropy and bond alternation in a frustrated ferromagnetic spin-1/2 chain, *Phys. Rev. B* **101**, 224439 (2020).
- [17] G. Meunier, J. Darriet, and J. Galy, L'oxyde double TeVO_4 II. Structure cristalline de TeVO_4 - β -relations structurales, *J. Solid State Chem.* **6**, 67 (1973).
- [18] M. Pregelj, A. Zorko, O. Zaharko, H. Nojiri, H. Berger, L. Chapon, and D. Arčon, Spin-stripe phase in a frustrated zigzag spin-1/2 chain, *Nat. Commun.* **6**, 7255 (2015).
- [19] M. Pregelj, A. Zorko, M. Gomilšek, M. Klanjšek, O. Zaharko, J. White, H. Luetkens, F. Coomer, T. Ivek, D. Góngora, H. Berger, and D. Arčon, Elementary excitation in the spin-stripe phase in quantum chains, *npj Quantum Mater.* **4**, 22 (2019).
- [20] M. Pregelj, A. Zorko, D. Arčon, M. Klanjšek, O. Zaharko, S. Krämer, M. Horvatić, and A. Prokofiev, Thermal effects versus spin nematicity in a frustrated spin-1/2 chain, *Phys. Rev. B* **102**, 081104(R) (2020).
- [21] F. Weickert, N. Harrison, B. L. Scott, M. Jaime, A. Leitmäe, I. Heinmaa, R. Stern, O. Janson, H. Berger, H. Rosner, and A. A. Tsirlin, Magnetic anisotropy in the frustrated spin-chain compound $\beta\text{-TeVO}_4$, *Phys. Rev. B* **94**, 064403 (2016).
- [22] W. W. Simmons, W. J. O'Sullivan, and W. A. Robinson, Nuclear spin-lattice relaxation in dilute paramagnetic sapphire, *Phys. Rev.* **127**, 1168 (1962).
- [23] A. M. Clogston, V. Jaccarino, and Y. Yafet, Interpretation of knight shifts and susceptibilities of transition metals: Platinum, *Phys. Rev.* **134**, A650 (1964).
- [24] A. Pelissetto and E. Vicari, Critical phenomena and renormalization-group theory, *Phys. Rep.* **368**, 549 (2002).
- [25] P. M. Chaikin and T. C. Lubensky, *Principles of Condensed Matter Physics* (Cambridge University Press, Cambridge, England, 2000), Vol. 1.
- [26] A. Saúl and G. Radtke, Density functional approach for the magnetism of $\beta\text{-TeVO}_4$, *Phys. Rev. B* **89**, 104414 (2014).
- [27] M. Pregelj, O. Zaharko, U. Stuhr, A. Zorko, H. Berger, A. Prokofiev, and D. Arčon, Coexisting spinons and magnons in frustrated zigzag spin-1/2 chain compound $\beta\text{-TeVO}_4$, *Phys. Rev. B* **98**, 094405 (2018).
- [28] A. D. Bain and M. Khasawneh, From NQR to NMR: The complete range of quadrupole interactions, *Concepts Magn. Reson., Part A* **22A**, 69 (2004).
- [29] M. Pregelj, P. Jeglič, A. Zorko, O. Zaharko, T. Apih, A. Gradišek, M. Komelj, H. Berger, and D. Arčon, Evolution of magnetic and crystal structures in the multiferroic $\text{FeTe}_2\text{O}_5\text{Br}$, *Phys. Rev. B* **87**, 144408 (2013).
- [30] F. Aimo, S. Krämer, M. Klanjšek, M. Horvatić, C. Berthier, and H. Kikuchi, Spin Configuration in the 1/3 Magnetization Plateau of Azurite Determined by NMR, *Phys. Rev. Lett.* **102**, 127205 (2009).
- [31] M. Pregelj, O. Zaharko, M. Herak, M. Gomilšek, A. Zorko, L. C. Chapon, F. Bourdarot, H. Berger, and D. Arčon, Exchange anisotropy as mechanism for spin-stripe formation in frustrated spin chains, *Phys. Rev. B* **94**, 081114(R) (2016).
- [32] S. Zumer and R. Blinc, Nuclear spin-lattice relaxation in incommensurate systems, *J. Phys. C: Solid State Phys.* **14**, 465 (1981).
- [33] R. Blinc, Magnetic resonance and relaxation in structurally incommensurate systems, *Phys. Rep.* **79**, 331 (1981).
- [34] T. Moriya, Nuclear magnetic relaxation in antiferromagnetics, *Prog. Theor. Phys.* **16**, 23 (1956).
- [35] M. Horvatić and C. Berthier, NMR studies of low-dimensional quantum antiferromagnets, in *High Magnetic Fields*, Lecture Notes in Physics, edited by C. Berthier, L. P. Lévy, and G. Martinez (Springer, Berlin, 2002), Vol. 595, pp. 191–210.
- [36] Y. Tokunaga, D. Aoki, H. Mayaffre, S. Krämer, M.-H. Julien, C. Berthier, M. Horvatić, H. Sakai, S. Kambe, and S. Araki, Reentrant Superconductivity Driven by Quantum

- Tricritical Fluctuations in URhGe: Evidence from ^{59}Co NMR in $\text{URh}_{0.9}\text{Co}_{0.1}\text{Ge}$, *Phys. Rev. Lett.* **114**, 216401 (2015).
- [37] H. Mayaffre, M. Horvatić, C. Berthier, M.-H. Julien, P. Ségransan, L. Lévy, and O. Piovesana, NMR Evidence for a “Generalized Spin-Peierls Transition” in the High-Magnetic-Field Phase of the Spin Ladder $\text{Cu}_2(\text{C}_5\text{H}_7\text{N}_2)_2\text{Cl}_4$, *Phys. Rev. Lett.* **85**, 4795 (2000).
- [38] M. Jeong, H. Mayaffre, C. Berthier, D. Schmidiger, A. Zheludev, and M. Horvatić, Magnetic-Order Crossover in Coupled Spin Ladders, *Phys. Rev. Lett.* **118**, 167206 (2017).
- [39] D. Beeman and P. Pincus, Nuclear spin-lattice relaxation in magnetic insulators, *Phys. Rev.* **166**, 359 (1968).